HOSTED BY

ELSEVIER

Available online at www.sciencedirect.com

ScienceDirect

International Soil and Water Conservation Research 3 (2015) 28–41

www.elsevier.com/locate/iswcr

Finite element method for one-dimensional rill erosion simulation on a curved slope

Lijuan Yan[a], Tingwu Lei[b,*], Jing Zhang[b], Qingwen Zhang[c], Liqin Qu[d]

[a]*Bureau of Comprehensive Development, Ministry of Water Resources, Beijing 100053, PR China*

[b]*Key Laboratory of Modern Precision Agriculture Integration Research, College of Hydraulic and Civil Engineering, China Agricultural University, Beijing 100083, PR China*

[c]*Institute of Environment and Sustainable Development in Agriculture, CAAS, Beijing 100081, PR China*

[d]*International Research and Training Center on Erosion and Sedimentation, Beijing 100048, PR China*

Received 22 January 2015; received in revised form 20 February 2015; accepted 21 February 2015

Available online 13 March 2015

Abstract

Rill erosion models are important to hillslope soil erosion prediction and to land use planning. The development of rill erosion models and their use has become increasingly of great concern. The purpose of this research was to develop mathematic models with computer simulation procedures to simulate and predict rill erosion. The finite element method is known as an efficient tool in many other applications than in rill soil erosion. In this study, the hydrodynamic and sediment continuity model equations for a rill erosion system were solved by the Galerkin finite element method and Visual C++ procedures. The simulated results are compared with the data for spatially and temporally measured processes for rill erosion under different conditions. The results indicate that the one-dimensional linear finite element method produced excellent predictions of rill erosion processes. Therefore, this study supplies a tool for further development of a dynamic soil erosion prediction model.

Keywords: Finite element method; Simulation; Rill erosion; Dynamics; Galerkin

1. Introduction

Soil eroded by shallow water flows such as over land or in-rill flow is a critical component of the erosion system on upland areas. The erosion processes of sediment detachment, transport, and deposition on hillslope areas are complex and interactive. This has been of great interest to mathematical and computer modelers for upland erosion modeling. A number of process-based dynamic models have been developed to better understand and model the processes of runoff and soil erosion under different situations. The water erosion prediction project (WEPP) model (Ascough, Baffaut, Nearing, & Liu, 1997; Flanagan & Nearing, 1995), European soil erosion (EuroSEM) model (Morgan, Quinton, & Rickson, 1992), the areal nonpoints source watershed environment response simulation (ANSWERS) model (Beasley, Huggins, & Monke, 1980), the Limburg soil erosion model (LISEM) (De Roo,

*Correspondence to: China Agricultural University, Qinghua Donglu, Beijing 100083, PR China. Fax: +86 10 6273 6367.

E-mail address: leitingwu@cau.edu.cn (T. Lei).

Peer review under responsibility of IRTCES and CWPP.

http://dx.doi.org/10.1016/j.iswcr.2015.03.001

Offermans, & Cremers, 1996), Griffith University Erosion System Template (GUEST) (Misra & Rose, 1996) are but some examples. However, most of the models are either empirical or using Finite Difference Method (FDM) to solve the mathematic equations. Model performances are either not efficient or are difficult to deal with complex boundary conditions as associated with FDM. Furthermore, model parameters are often, if not impossible, difficult to directly measure to present the actual physical properties (Lane, Shirley, & Singh, 1988).

Generally, soil erosion occurs on a three-dimensional (3-D) surface. But soil erosion behavior in a rill could to some extent be well described with a one-dimensional (1-D) model. And the dynamic process of soil erosion along a streamline of overland flow could be approximated with a one-dimensional model for the purpose of understanding the basic mechanics behind the complicated phenomenon. The governing equations are a set of partial differential equations involved in the hydrologic erosion processes. Numerical techniques do not need to make as many assumptions as required for analytic solutions. The driving force that is the rainfall excess term can vary with time and space (Lane et al., 1988; Sharda, Singh, Sastry, & Dhruvanarayana, 1994). Numerical methods such as the finite difference method (FDM) and the finite element method (FEM) are employed to solve these equations. Finite element techniques are generally recognized to have significant advantages over finite difference procedures for irregularly shaped flow regions (Zienkiewics, Taylor, & Zhu, 2013) FEM is now widely used to solve a variety of important problems in the field of soil science and groundwater hydrology. A lot of works has been accomplished in early studies (Bralts & Segerlind, 1985; Guymon, 1972; Jayawardena & White, 1977; Ross, Contractor, & Shanholtz, 1979; Taylor, Al-Mashidani, & Davis, 1974). Recently, Celia, Bouloutas, and Zarba (1990) stated that numerical approximations based on different forms of the governing partial differential equation can lead to significantly different results for unsaturated flow problems. A finite element model simulating runoff and soil erosion from agricultural lands has been developed by Sharda and Nearing (1999). The sediment continuity equation was solved employing a fully implicit scheme for time integration. The complete Yalin's equation (Yalin, 1977) was used to simulate sediment transport capacity (Sharda et al., 1994; Sharda & Nearing, 1999; Sharda & Singh, 1994). Jaber and Mohtar (2002) evaluate the stability and accuracy of finite element schemes for the one-dimensional kinematic wave solution. They believed the lumped scheme considerably reduces oscillations without significant reduction in the overall solution accuracy. A kinematic wave based distributed watershed model using the finite element method, GIS and remotely sensed data has been reported by Venkata, Eldho, Rao, and Chithra (2008). This model could simulate hydrographs reasonably well at the outlet of the watershed.

The purposes of this study are: to develop the mathematic models for one-dimensional rill soil erosion on hillslope, including the hydrodynamics of shallow water flow along rills on the curved slopes, the soil detachment/deposition and transportation; to develop numerical algorithms and the FEM formulations for simulating the spatial and temporal processes; and, to validate the procedures by comparing the computed results with laboratory experimental data.

2. The mathematical models

Basic assumptions for deriving the mathematic model for soil erosion from 1-D rill under the impact of water flow are: (1) the water is very shallow, compared with the length; (2) velocity in the vertical direction is a uniformly distributed flow profile and (3) Velocity is that of depth-averaged. Based on those assumptions the mathematic models for rill erosion are given as the following.

2.1. Hydrodynamic models

The derivations of the continuity and momentum equations for overland and channel flow can be found in a number of references (Ascough et al., 1997; Kibler & Woolhiser, 1970; Lei, Nearing, Haghighi, & Bralts, 1998; Sharda & Nearing, 1999; Tsai & Yang, 2005). For mass conservation, the governing equation is written as

$$\frac{\partial h}{\partial t} + \frac{\partial (uh)}{\partial x} = \sigma \tag{1}$$

while momentum conservation equation given as

$$\frac{\partial u}{\partial t}+u\frac{\partial u}{\partial x}+g\frac{\partial h}{\partial x}=-\frac{u\sigma}{h}-g\left(\frac{S_x}{\sqrt{1+S_x^2}}+S_{fx}\right)+F_{Cn}n_x \tag{2}$$

where $x(m)$ is the Cartesian coordinates, $t(s)$ is the time, $h(x, t)$ (m) is the depth of flow measured in the vertical direction, $u(x, t)$ (m s^{-1}) is the depth-averaged velocity in the x-direction, $\sigma(x, t)$ (m s^{-1}) is the excessive rainfall intensity, g (9.82 m t^{-2}) is acceleration due to gravity, S_x (mm^{-1}) is the geographic slope, S_{fx} (mm^{-1}) is the (hydraulic) friction slope, may be obtained as

$$S_{fx}=\left(\frac{u}{C}\right)^2\frac{1}{h} \tag{3}$$

in which C is Chezy's C, a factor of flow resistance, given by

$$C=\sqrt{\frac{8g}{f}} \tag{4}$$

f is the Darcy–Weisbach hydraulic frictional coefficient.

$\vec{F_C}$ is the contribution made by centrifugal accelerations, caused by the curved soil surface. This force can be viewed as the force acting on the fluid by the soil body to force the fluid to flow along a curved streamline instead of in a straight line, or viewed as the inertial force of the fluid, as the way gravity force acts on the fluid. It is normally neglected.

2.2. Sediment transport model

According to the mass conservation of sedimentation and Frick's law, we have sediment transport model as (Lei et al., 1998)

$$c\sigma+h\frac{\partial c}{\partial t}+hu\frac{\partial c}{\partial x}=\frac{\partial}{\partial x}\left(hD_H\frac{\partial c}{\partial x}\right)+S_{ss} \tag{5}$$

where c (kg m^{-3}) is sediment concentration in the flow.

D_H (m^2 s^{-1}) is a hydraulic diffusive coefficient. Many different D_H values were tried so as to help determine if D_H is significantly important in the rill erosion process and what value should be used (Lei et al., 1998). They found that 0.01–0.1 seems good enough in many situations. A value of 0.05 for D_H was used in this study.

$S_{ss}(x,t)$ (kg m^{-2} s^{-1}) is the sediment source/sink term. It is equal to rill detachment rate D_r (kg m^{-2} s^{-1}) in the rill erosion system. It has been computed following rill erosion prediction in the Water Erosion Prediction Project (WEPP) model (Ascough et al., 1997):

$$D_r=K_r(\tau-\tau_c)\left[1-\frac{G}{T_c}\right] \tag{6}$$

where T_c (kg s^{-1} m^{-1}) in Eq. (6) is the sediment transport capacity. It is defined by the following equation (Lei, Zhang, Zhao, & Tang, 2001):

$$T_c=a+bS+cQ \tag{7}$$

where S (deg) is the slope and Q (l/min) is the flow rate. For silty–clay (loess) soil, $a=-0.3109$, $b=0.01718$ and $c=0.1203$. τ (N m^{-2}) is the shear stress of the flowing water. According to the principles of hydrodynamics, shear stress of water flow is equal to the gravitational component along the flow direction. Thus it can be expressed as (Gilley, Elliot, Laflen, & Simanton, 1993)

$$\tau=\gamma sh=\gamma s\frac{Q}{uw} \tag{8}$$

where g (9820 N m^{-3}) is specific gravity of water, s (sin(a)) is hydraulic slope, $a(^\circ)$ is slope in degrees; u (m s^{-1}) is averaged velocity, (N m^{-2}) is the critical shear stress of soil. K_r (kg N^{-1} s^{-1}) is the rill erodibility parameter.

A rational method for determining the soil erodibility and critical shear stress of rill erosion under concentrated flow is advanced by Zhang, Lei, Pan, and Gao (2004). From his work, soil erodibility of a typical loess soil was 0.3211 ± 0.0003 kg/N s, the critical shear stresses τ_c increase a little with the slope gradients, namely 3.19 N/m^2, 3.94 N/m^2, 4.14 N/m^2, 4.38 N/m^2, 4.62 N/m^2 under 5°, 10°, 15°, 20°, 25°, respectively.

3. Derivation of finite element equation

3.1. The system of linear elements

A one-dimensional linear element was used to formulate the FEM solution in this study. The typical linear element and nodal structure used are shown in Fig. 1. In the method of weighted residuals, the continuous function □ is replaced by a finite series approximation □. A standard linear interpolation scheme is used. The approximation function □ may be written as

$$\psi \approx \phi = N_i\phi_i + N_j\phi_j = \begin{bmatrix} N_i, N_j \end{bmatrix} \begin{Bmatrix} \phi_i \\ \phi_j \end{Bmatrix} \tag{9}$$

where □$_i$ and □$_i$ are known values of the interpolation function □ at the element vertices, N_i and N_j are interpolation functions at node i and j, which depend upon the Cartesian coordinates (x,□) of the element vertices. Geometrically, interpolation functions are represented mathematically as

$$\begin{cases} [N] = [N_i, N_j.] \\ N_i = \frac{X_j - x}{X_j - X_i} = \frac{X_j - x}{L} \\ N_j = \frac{x - X_i}{X_j - X_i} = \frac{x - X_i}{L} \end{cases} \tag{10}$$

where X_i and X_j are the coordinates of the nodes, $L = X_j - X_i$, is the length of the element.

From Eq. (10), the derivative of N_i and N_j with respect to x (or s) is given as respectively

$$\frac{\partial N_i}{\partial x} = -\frac{1}{L} \tag{11a}$$

$$\frac{\partial N_j}{\partial x} = \frac{1}{L} \tag{11b}$$

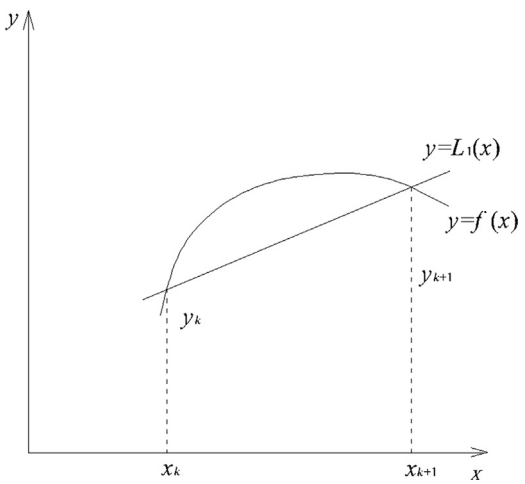

Fig. 1. The 1-D linear element.

The integral of polynomial function of shape functions over an element is determined by (Segerlind, 1976)

$$\int_L N_i{}^m(x)N_j{}^n(x)dx = \frac{m!n!}{(m+n+1)!}L \tag{12}$$

where m and n are exponents of the interpolation functions N_i, N_j.

3.2. Galerkin method

The Galerkin method was used for solving the one-dimensional hydrodynamic and sediment continuity equations. The detailed description and integral of finite element solution is given as follows.

Using operators, L_1, L_2, and L_3 (as defined in the following) to Eqs. (1), (2) and (5) yields

$$L_1(u,h) = \frac{\partial h}{\partial t} + \frac{\partial (uh)}{\partial x} - \sigma = 0 \tag{13}$$

$$L_2(u,h) = \frac{\partial u}{\partial t} + u\frac{\partial u}{\partial x} + g\frac{\partial h}{\partial x} + \frac{u\sigma}{h} + g\left(\frac{S_x}{\sqrt{1+S_x^2}} + S_{fx}\right) = 0 \tag{14}$$

$$L_3(u,h,c) = c\sigma + h\frac{\partial c}{\partial t} + hu\frac{\partial c}{\partial x} - \frac{\partial}{\partial x}\left(hD_H\frac{\partial c}{\partial x}\right) - D_r = 0 \tag{15}$$

For approximations, variable u, h, c, $\square$, S_x, $(\partial u/\partial t)$, $(\partial h/\partial t)$ and $(\partial c/\partial t)$ are given in the form of Eq. (9), which produce some errors or residuals, denoted with R_1, R_2, and R_3 as

$$\begin{cases} R_1 = L_1(u,h) \\ R_2 = L_2(u,h) \\ R_3 = L_3(u,h,c) \end{cases} \tag{16}$$

Galerkin weighted residual method requires that the integrals of these residuals by each shape (or weight) function be zero. The residual equation for element e takes the form as

$$\begin{Bmatrix} R_1^e \\ R_2^e \\ R_3^e \end{Bmatrix} = \int_L [N^e] \begin{bmatrix} \left(\frac{\partial h^e}{\partial t} + u^e\frac{\partial h^e}{\partial x} + h^e\frac{\partial u^e}{\partial x} - \sigma^e\right) \\ \left(\frac{\partial u^e}{\partial t} + u^e\frac{\partial u^e}{\partial x} + g\frac{\partial h^e}{\partial x} + \frac{\sigma^e u^e}{h^e} + g\left(\frac{S_x^e}{\sqrt{1+(S_x^e)^2}} + S_{fx}^e\right)\right) \\ \left(h^e\frac{\partial c^e}{\partial t} + h^e u^e\frac{\partial c^e}{\partial x} - \frac{\partial}{\partial x}\left(h^e D_H\frac{\partial c}{\partial x}\right) - D_r - c\sigma^e\right) \end{bmatrix} dl = 0 \tag{17}$$

where L (m) refers to the length of the element, $[N^e]$ and $\{R^e\}$ are the interpolation function and the nodal residuals associated with element e, respectively.

Eq. (17) can be integrated in the form of an ordinary differential equation as follows:

$$[C^e]\left\{\frac{\partial \varphi}{\partial t}\right\} + [K^e]\{\varphi\} = \{f^e\} \tag{18}$$

where $\{\square\}$ is $\{h\}$,$\{u\}$ or $\{c\}$, and $[C^e]$, $[K^e]$ and $\{f^e\}$ are the capacitance matrix, the stiffness matrix, and the force vector in each equation and element, respectively

$$[C^e] = \begin{cases} \int_L [N^e]^T[N^e]dl \\ \int_L [N^e]^T[N^e]dl \\ \overline{h}^e\int_L [N^e]^T[N^e]dl \end{cases} \tag{19}$$

$$[K^e]=\begin{cases}\overline{u}^e\int_L[N^e]^T\frac{\partial[N^e]}{\partial x}dl+\overline{u}_x^e\int_L[N^e]^T[N^e]dl\\ \overline{u}^e\int_L[N^e]^T\frac{\partial[N^e]}{\partial x}dl+\frac{\overline{\sigma}^e}{\overline{h}^e}\int_L[N^e]^T[N^e]dl\\ \overline{u}^e\overline{u}^e\int_L[N^e]^T\frac{\partial[N^e]}{\partial x}dl+\overline{h}^e\overline{D}_H^e\int_L\frac{\partial[N^e]^T}{\partial x}\frac{\partial[N^e]}{\partial x}dl+\overline{\sigma}^e\int_L[N^e]^T[N^e]dl\end{cases}\tag{20}$$

$$\{\{f^e\}\}=\begin{cases}\left(\int_L[N^e]^T[N^e]dl\right)\{\sigma^e\}\\ -g\left(\int_L[N^e]^T\frac{\partial[N^e]}{\partial x}dl\right)\{h^e\}-g\left(\int_L[N^e]^T[N^e]dl\right)\left\{\frac{1}{\sqrt{1+(\overline{S}_x^e)^2}}\{S_x\}+S_{fx}^e\left\{u_{t-\Delta t}^e\right\}\right\}\\ \left(\int_L[N^e]^T[N^e]dl\right)\{D_r{}^e\}\end{cases}\tag{21}$$

Herein, u_x^e is the derivative of u^e, S_{fx}^e and $\overline{S}_{fx}^e$ is determined by

$$S_{fx}^e=u^e\overline{S}_{fx}^e=u^e\frac{1}{\overline{C}^2}\frac{\overline{u}^e}{\overline{h}^e}\tag{22}$$

$$\overline{S}_{fx}^e=\frac{1}{C^2}\frac{\overline{u}^e}{\overline{h}^e}\tag{23}$$

where $\overline{u}^e$, $\overline{h}^e$, $\overline{C}^e$, $\overline{\sigma}^e$, $\overline{D_H}^e$, $\overline{s_x}^e$ and $\overline{s_{fx}}^e$ are the averages of the corresponding variables within the element e, $\overline{u_x}^e$ is the averages of the derivative of the velocity within the element.

3.3. Numerical formulations

Using Eqs. (11a), (11b) and (12), the related integrals necessary for the FEM formulations are estimated as the following:

$$\int_L[N^e]^T[N^e]dx=\int_L\begin{bmatrix}N_i{}^e\\ N_j{}^e\end{bmatrix}\begin{bmatrix}N_i{}^e & N_j{}^e\end{bmatrix}dx=\frac{L}{6}\begin{bmatrix}2 & 1\\ 1 & 2\end{bmatrix}\tag{24}$$

$$\int_L[N^e]^T\frac{\partial[N^e]}{\partial x}dx=\int_L\begin{bmatrix}N_i^e\\ N_j^e\end{bmatrix}\frac{\partial\begin{bmatrix}N_i^eN_j^e\end{bmatrix}}{\partial x}dx=\frac{1}{2}\begin{bmatrix}-1 & 1\\ -1 & 1\end{bmatrix}\tag{25}$$

$$\int_L\frac{\partial[N^e]^T}{\partial x}\frac{\partial[N^e]}{\partial x}dx=\int_L\frac{\partial\begin{bmatrix}N_i^e\\ N_j^e\end{bmatrix}}{\partial x}\frac{\partial\begin{bmatrix}N_i^eN_j^e\end{bmatrix}}{\partial x}dx=\frac{1}{L}\begin{bmatrix}1 & -1\\ -1 & 1\end{bmatrix}\tag{26}$$

So Eqs.(19)–(21), can then be computed as follows:

$$[C^e]=\begin{cases}\frac{L}{6}\begin{bmatrix}2 & 1\\ 1 & 2\end{bmatrix}\\ \frac{L}{6}\begin{bmatrix}2 & 1\\ 1 & 2\end{bmatrix}\\ \frac{\overline{h}L}{6}\begin{bmatrix}2 & 1\\ 1 & 2\end{bmatrix}\end{cases}\tag{27}$$

$$[K^e]=\begin{cases}\frac{\overline{u}^e}{2}\begin{bmatrix}-1 & 1\\ -1 & 1\end{bmatrix}+\frac{\overline{u_x}^e L}{6}\begin{bmatrix}2 & 1\\ 1 & 2\end{bmatrix}\\ \frac{\overline{u}^e}{2}\begin{bmatrix}-1 & 1\\ -1 & 1\end{bmatrix}+\frac{\overline{\sigma}^e L}{6\overline{h}^e}\begin{bmatrix}2 & 1\\ 1 & 2\end{bmatrix}\\ \frac{\overline{h}^e\overline{u}^e}{2}\begin{bmatrix}-1 & 1\\ -1 & 1\end{bmatrix}+\frac{\overline{h}^e\overline{D_H}^e}{L}\begin{bmatrix}1 & -1\\ -1 & 1\end{bmatrix}+\frac{\overline{\sigma}^e L}{6}\begin{bmatrix}2 & 1\\ 1 & 2\end{bmatrix}\end{cases} \tag{28}$$

$$\{f^e\}=\begin{cases}\frac{L}{6}\begin{bmatrix}2 & 1\\ 1 & 2\end{bmatrix}\{\sigma^e\}\\ -\frac{g}{2}\begin{bmatrix}-1 & 1\\ -1 & 1\end{bmatrix}\{h^e\}-\frac{gL}{6}\begin{bmatrix}2 & 1\\ 1 & 2\end{bmatrix}\left\{\frac{1}{\sqrt{1+(\overline{S}_x^e)^2}}\{S_x\}+S_{fx}^e\{u_{t-\Delta t}^e\}\right\}\\ \frac{L}{6}\begin{bmatrix}2 & 1\\ 1 & 2\end{bmatrix}\{D_r{}^e\}\end{cases} \tag{29}$$

3.4. Approximation of the time derivatives

The system of equations expressed by Eq. (18) is a system of ordinary differential equations with respect to time. The so called time marching integral method can be used to obtain the solutions for different time steps. For this purpose, finite difference in time is adopted.

For a function $\square(t)$, the following holds:

$$\frac{d\phi(\xi)}{dt}=\frac{\phi(t+\Delta t)-\phi(t)}{\Delta t} \tag{30}$$

$$\phi(\xi)=\phi(t)+(\xi-t)\frac{\phi(t+\Delta t)}{\Delta t}=(1-\theta)\phi(t)+\theta\phi(t+\Delta t) \tag{31}$$

where t is time point, $\square$ is some point on the interval t to $t+\Delta t$, Δt is the time step length.

$$\theta=\frac{\xi-t}{\Delta t} \tag{32}$$

Applying Eqs. (30)–(32) in Eq. (18) yields

$$[C^e]\frac{\{\phi\}_{t+\Delta t}-\{\phi\}_t}{\Delta t}+(1-\theta)[K^e]\{\phi\}_t+\theta[K^e]\{\phi\}_{t+\Delta t}=\{f^e\}_t \tag{33}$$

Rearranging the equation above yields

$$([C^e]+\theta\Delta t[K^e])\{\phi\}_{t+\Delta t}=([C^e]-(1-\theta)\Delta t[K^e])\{\phi\}_t+\Delta t\{f^e\}_t \tag{34}$$

Giving initial conditions, combined with appropriate boundary conditions, Eq. (34) gives the desired solutions for u, v and h at nodes and at different time steps. Eq. (34) can be written as

$$[A^e]\{\phi^e\}_{t+\Delta t}=\{B^e\} \tag{35}$$

where

$$\begin{aligned}[A^e]&=([C^e]+\theta\Delta t[K^e])\\ \{B^e\}&=([C^e]-(1-\theta)\Delta t[K^e])\{\phi\}_t+\Delta t\{f^e\}_t\end{aligned} \tag{36}$$

And we have the system of equations for the element (e) as

$$[A]\{\phi\}_{t+\Delta t}=\{B\} \tag{37}$$

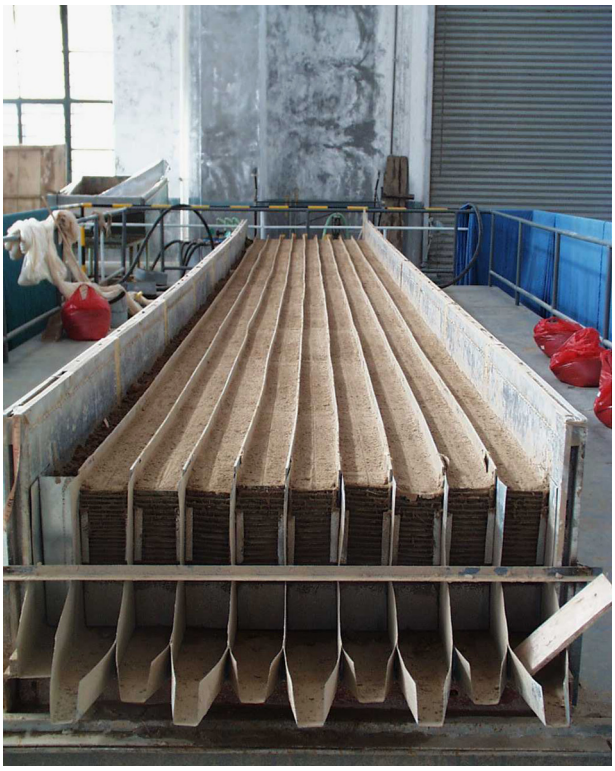

Fig. 2. The experimental equipment and its layout.

Assembling the local matrices $[A^e]$ and vectors $\{B^e\}$ ($e=1, 2,\ldots, N$) directly with the following equations, obtains the matrix $[A]$ and vector $\{B\}$ needed in Eq. (37):

$$[A] = \sum_{e=1}^{N} [A^e] \tag{38}$$

$$[B] = \sum_{e=1}^{N} [B^e] \tag{39}$$

In this way, we do not need to store the global matrices $[C]$ and $[K]$ before getting the matrix $[A]$ and vector $\{B\}$ by multiplications with Eq. (36). So the storage saving would be expected by storing only one global matrix $[A]$ instead of storing two global matrices $[C]$ and $[K]$.

4. Model application and discussion

4.1. Experimental setup

4.1.1. Experiment for sediment concentration change with time

To validate the feasibility of the method advanced above, experiment data with silt-clay (loess soil) from Yao (2006) were used. The experiments were conducted with a flume about 8 m long and 1 m wide which was subdivided into strips of 8 by 0.1 m to imitate erosion from rills. The treatments involved two slopes (15° and 25°) and two flow rates (2 and 4 L/min). The regulated water flow was introduced into the flume from the upper end. Three replicates were adopted. The experiment lasted 100 s. Metal outlets for collecting samples of runoff and sediment were connected at the lower end of each strip every 20 s.

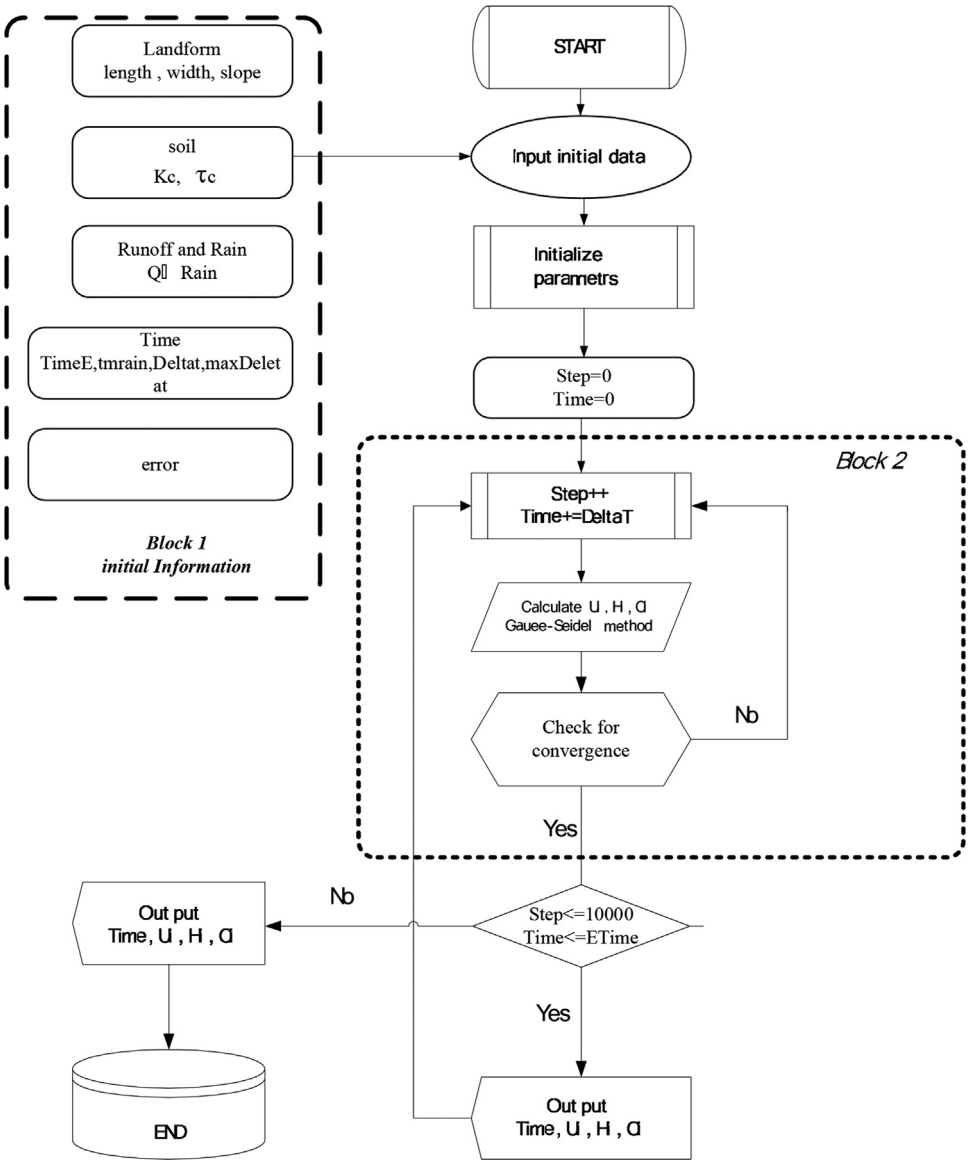

Fig. 3. Flow chart.

Experimental data from a previous study (Lei et al., 2001) with silt-clay (loess soil) was used to evaluate the impacts of model parameters on rill erosion processes. The experiments were made with a flume of 8 m long and 1 m wide which was divided into sections of 8×0.1 m^2 (Fig. 2). The experiments involved five slopes (5°, 10°, 15°, 20°, and 25°), 9 slope lengths (0.5, 1, 2, 3, 4, 5, 6, 7, 8 m), and three flow rates (2, 4, and 8 L/min). Numerical simulations were made on the same conditions as the experiments for 15° and 25°, 2 L/min and 4 L/min cases for model verification. Simulated sediment concentrations along the rills were compared with those from the experiments.

4.2. Calculation procedures

The flow domain for the overland flow has been divided into N linear elements with nodes at x_1, x_2,…, x_{N+1}, where $x_1 = 0$ and $x_{N+1} = L$.

As shown in the flow chart (Fig. 3), in Block 1, the input includes rill information, initial conditions and boundary conditions, widths, error limits for velocity, water depth and sediment concentration, soil information such as, rill

erodibility, critical shear stress of soil, the rainfall duration etc. Block 2 simulates the period of the runoff and rain, the velocity, water depth and sediment concentration, by implementing the following procedures:

- Calculate velocity and water depth in Eqs. (1) and (2);
- Determine the transport capacity, Eq. (7);
- Compute detachment rate by Eq. (6);
- Solve the sediment continuity equation for sediment concentration, Eq. (5);
- The convergence criteria in Block 2 are set as:

$$\max_{0 \le i \le N+1} \frac{\left|\varphi_i^{(k+1)} - \varphi_i^k\right|}{\overline{\varphi_i}} \le \delta \tag{40}$$

where φ is h, u, or c; k is the time step; σ is the error limit.

4.3. Result and discussion

4.3.1. Comparison of simulated and experimental results for sediment concentration change with time

The samples of sediment concentration from experimentally measured and simulated results are graphically shown in Fig. 4a–d. The simulated and experimental results do not change much during the measurement time durations

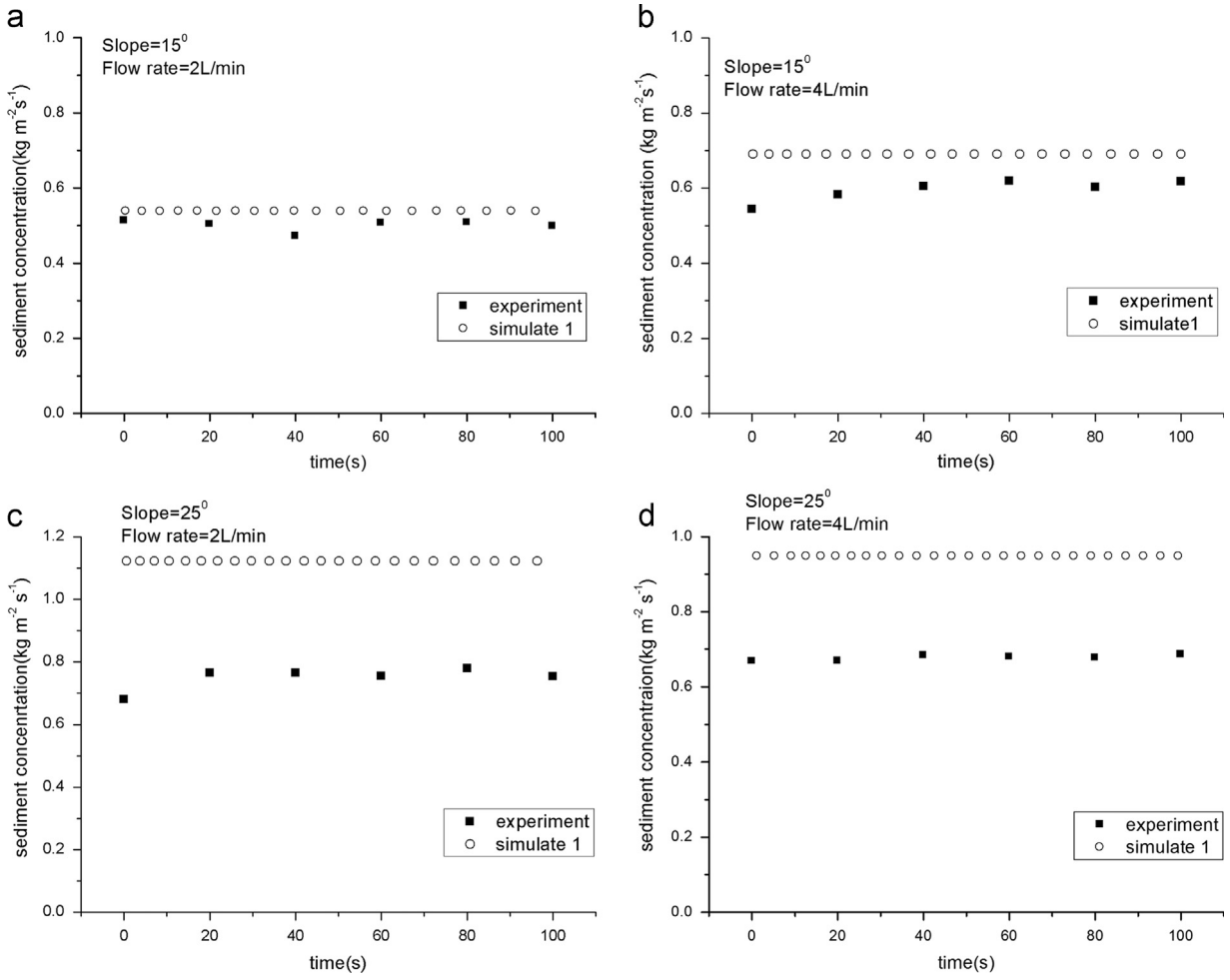

Fig. 4. Comparisons of simulated and experimental for sediment concentration change with time.

because the sediment concentrations obtained at the end of the rill reached their transport capacities. Therefore they were almost constant with time.

The observed and the numerically simulated results agreed very well, except for those at 25°. There are two reasons for this. One reason was the transport capacity estimated from the experiments was based on different slopes and flow rates. According to previous experiment work, the predicted Transport Capacity is lower than the experimental at 15° and higher at 25° (Lei et al., 2001). So the error was brought into this study. Since transport capacity controls the maximum possible sediment concentration, the simulated is lower than the measured at 15° and higher at 25°. There is another reason that may need to be taken into account. The transport capacity function is based on the soil that is not exactly at the same density as that used in Yao's experiments. The soil density of Yao's experiments was higher than that in Zhang's experiments, which should have lowered erodability. Reasonably, the measured results are all lower than Zhang's. Under these two effects above, the simulated data is close to experimental data at 15°, but lower at 25°. In order to explain that this error does not come from the numerical method and procedure, but from the transport capacity formula, a new function was fitted based on Yao's experimental data with regressed coefficients as $a=-0.137$, $b=0.006$ and $c=0.108$. Simulations were also made with these newly determined data, as shown in Fig. 5a–d. The measured and predicted sediment concentrations agreed qualitatively well. It indicated that the numerical algorithm and the FEM formulations for simulating the erosion processes were correct.

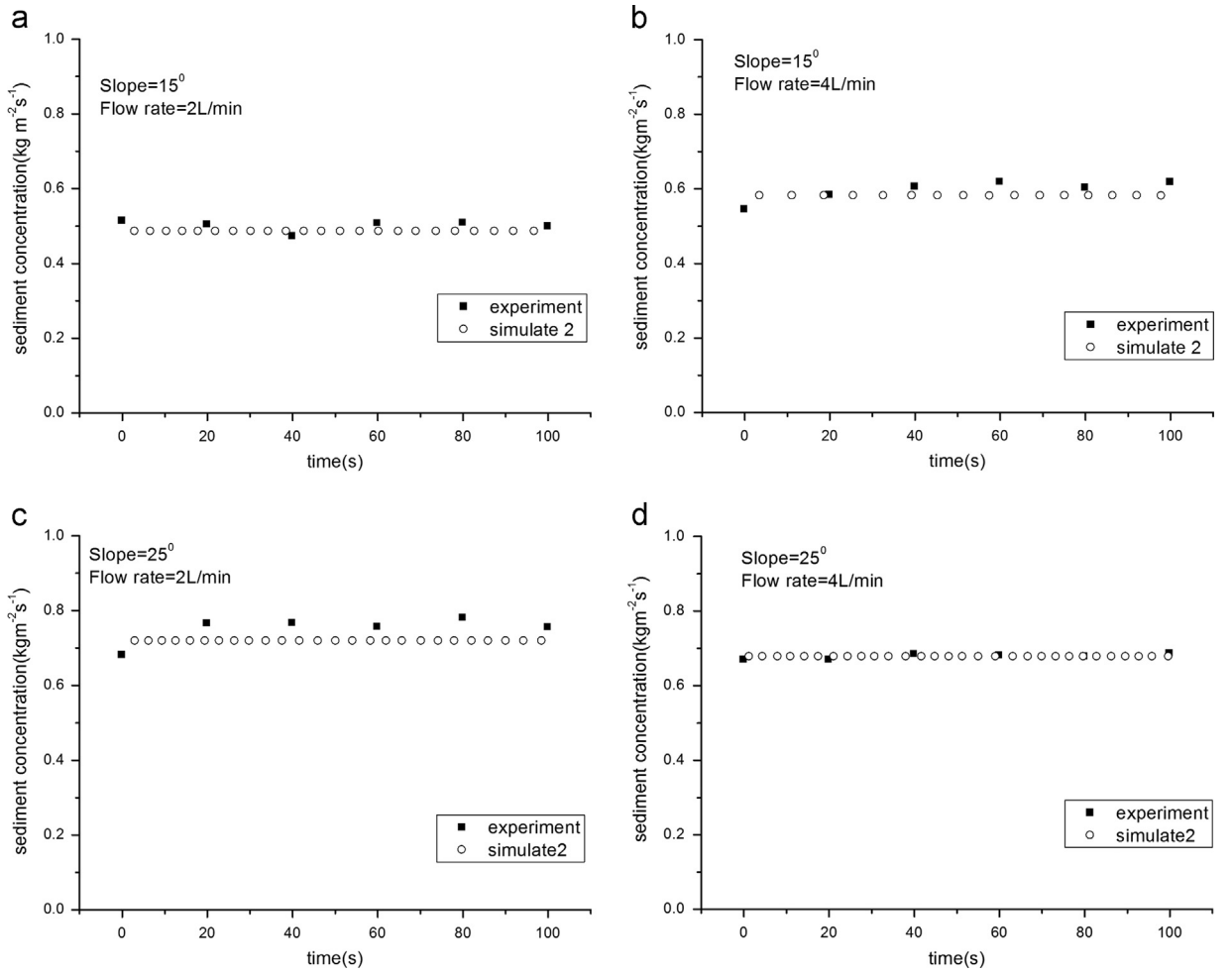

Fig. 5. Modify transport capacity then comparisons of simulated and experimental date for sediment concentration change with time.

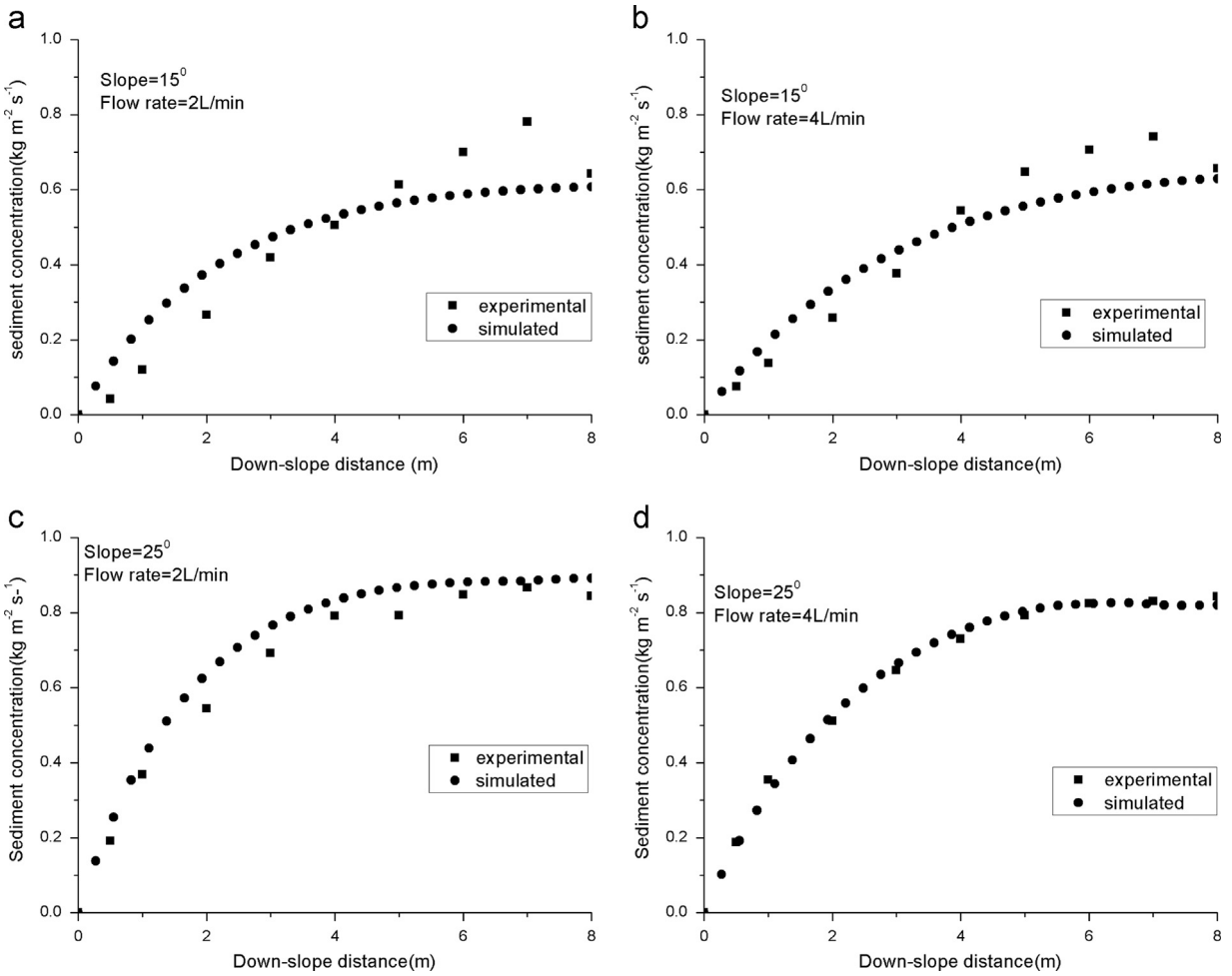

Fig. 6. Comparison of simulated and experimental for sediment concentration change with rill length.

4.3.2. Comparison of simulated and experimental results for sediment concentration change with rill length

The simulated sediment concentrations along rills under different slope and flow rate conditions were compared with Zhang's experimental data (Zhang, 2004) under the same conditions, as shown in Fig. 6a and b. The figures indicate very good agreement of the simulated and experimental results. The sediment concentration increases with rill length, but the increase rate diminished gradually. It increases until it reaches transport capacity. When constant flow rate is introduced into the rill, water depth and velocity after some period of time both become constant and uniform, and hence sediment transport capacity is also uniform and constant with time. The results indicate that both the mathematical models and the numerical algorithms of the finite element method as well as the computational procedure codes were correct.

5. Conclusions

A mathematical model based on the hydrodynamic and sediment transport theory was implemented in a computer model for simulating rill erosion processes. The model was based on applying the Galerkin formulation of the finite element method. The model simulates the velocity, depth and sediment concentration of the rill flow. Sediment concentration was verified then validated by comparing its output results with the laboratory observations of the flume experimental system. The results indicate that the model can serve as an effective tool in predicting the process of rill erosion.

From the results, it can be concluded that the finite element method can be successfully used to predict rill erosion. It was demonstrated that the one-dimensional linear finite element method produced excellent predictions for the test. The general applicability of the current version of the model and the scope for future development are valuable issues requiring considerable discussion.

Acknowledgments

This research was financially supported by the National Natural Science Foundation of China under Project no. 40635027, and No. 51321001.

References

Ascough, J., Baffaut, C., Nearing, M. A., & Liu, B. Y. (1997). The WEPP watershed model: I. Hydrology and erosion. *Transactions of the ASAE*, *40*(4), 921–933.

Beasley, D. B., Huggins, L. F., & Monke, E. J. (1980). ANSWERS: A model for watershed planning. *Transactions of the ASAE—American Society of Agricultural Engineers*, *23*, 938–944.

Bralts, V. F., & Segerlind, L. J. (1985). Finite element analysis of drip irrigation submain units. *Transactions of the ASAE—American Society of Agricultural Engineers (USA)*, *28*(3), 809–814.

Celia, M. A., Bouloutas, E. T., & Zarba, R. L. (1990). A general mass-conservative numerical solution for the unsaturated flow equation. *Water Resources Research*, *26*(7), 1483–1496.

De Roo, P. J., Offermans, R., & Cremers, N. (1996). A single-event physically-based hydrological and soil erosion model for drainage basins. II: Sensitivity analysis, validation and application. *Hydrological Processes*, *10*(8), 1119–1126.

Flanagan, D. C., & Nearing, M. A. (Eds.). (1995). West Lafayette, Indiana: USDA-ARS National Soil Erosion Research Laboratory.

Gilley, J. E., Elliot, W. J., Laflen, J. M., & Simanton, J. R. (1993). Critical shear stress and critical flow rates for initiation of rilling. *Journal of Hydrology*, *142*(1), 251–271.

Guymon, G. L. (1972). *Application of the finite element method for the simulation of surface water transport problems* (Doctoral dissertation). Anchorage, AK: Institute of Water Resources, University of Alaska.

Jaber, F. H., & Mohtar, R. H. (2002). Stability and accuracy of finite element schemes for the one-dimensional kinematic wave solution. *Advances in Water Resources*, *25*(4), 427–438.

Jayawardena, A. W., & White, J. K. (1977). A finite element distributed catchment model, I. Analytical basis. *Journal of Hydrology*, *34*(3), 269–286.

Kibler, D. F., & Woolhiser, D. A. (1970). *The kinematic cascade as a hydrologic model. Hydrology paper no. 39*. Fort Collins, Colorado: Colorado State University.

Lane, L. J., Shirley, E. D., & Singh, V. P. (1988). *Modelling Geomorphological Systems Chapter 10 Modelling Erosion On Hillslopes, M.G. Anderson*. New York: John Wiley&Sons Ltd.

Lei, T., Nearing, M. A., Haghighi, K., & Bralts, V. F. (1998). Rill erosion and morphological evolution: A simulation model. *Water Resources Research*, *34*(11), 3157–3168.

Lei, T. W., Zhang, Q., Zhao, J., & Tang, Z. (2001). A laboratory study of sediment transport capacity in the dynamic process of rill erosion. *Transactions of the ASAE*, *44*(6), 1537–1542.

Misra, R. K., & Rose, C. W. (1996). Application and sensitivity analysis of process-based erosion model GUEST. *European Journal of Soil Science*, *47*(4), 593–604.

Morgan, R., Quinton, J. N., & Rickson, R. J. (1992). *EUROSEM documentation manual*. Silsoe, UK: Silsoe College.

Ross, B. B., Contractor, D. N., & Shanholtz, V. O. (1979). A finite-element model of overland and channel flow for assessing the hydrologic impact of land-use change. *Journal of Hydrology*, *41*(1), 11–30.

Segerlind, L. J. (1976). *Applied finite element analysis*. New York: Wiley.

Sharda, V. N., Singh, S. R., Sastry, G., & Dhruvanarayana, V. V. (1994). A finite element model for simulating runoff and soil erosion from mechanically treated agricultural lands: 2. Field validation and applications. *Water Resources Research*, *30*(7), 2299–2310.

Sharda, V. N., & Nearing, M. (1999). *Finite element modeling of erosion on agricultural lands*. In Paper presented at the sustaining the global farm. Selected papers from the 10th international soil conservation organization meeting. West Lafayette, IN: Purdue University and the USDA-ARS National Soil Erosion Research Laboratory.

Sharda, V. N., & Singh, S. R. (1994). A finite element model for simulating runoff and soil erosion from mechanically treated agricultural lands: 1. Governing equations and solutions. *Water Resources Research*, *30*(7), 2287–2298.

Taylor, C., Al-Mashidani, G., & Davis, J. M. (1974). A finite element approach to watershed runoff. *Journal of Hydrology*, *21*(3), 231–246.

Tsai, T., & Yang, J. (2005). Kinematic wave modeling of overland flow using characteristics method with cubic-spline interpolation. *Advances in Water Resources*, *28*(7), 661–670.

Venkata, R. K., Eldho, T. I., Rao, E. P., & Chithra, N. R. (2008). A distributed kinematic wave—Philip infiltration watershed model using FEM, GIS and remotely sensed data. *Water Resources management*, *22*(6), 737–755.

Yalin, M. S. (1977). *Mechanics of sediment transport*. Oxford, U.K.: Pergamon.

Yao, C. (2006). *Experimental and model study on the coupled hillslope-rill water erosion processes* (Doctoral dissertation). Beijing: China Agriculture University.

Zhang, Q. W., Lei, T. W., Pan, Y. H., & Gao, P. L. (2004). Rational computational method of soil erodibility and critical shear stress from experiment data. *Journal of the Graduate School of the Chinese Academy of Sciences*, *21*, 468–475. (in Chinese).

Zhang, W. Q. (2004). *A systematic study on the model parameters of rill erosion and their relations with hydrodynmics* (Ph.D.). Yangling, Shaanxi: Chinese Academy of Scimence and Ministry of Education.

Zienkiewics, O. C., Taylor, R. L., & Zhu, J. Z. (2013). *The finite element method: Its basis and fundamentals* (7th ed.). Kidlington: Elsevier/Butterworth-Heinemann.